International Journal of Solids and Structures 51 (2014) 3012–3024

Contents lists available at ScienceDirect

International Journal of Solids and Structures

journal homepage: www.elsevier.com/locate/ijsolstr

Magnetoactive elastomers with periodic and random microstructures

Evan Galipeau [a], Stephan Rudykh [b,d], Gal deBotton [c,*], Pedro Ponte Castañeda [a]

[a] Department of Mechanical Engineering and Applied Mechanics, University of Pennsylvania, Philadelphia, PA 19104-6315, USA
[b] Department of Mechanical Engineering, Massachusetts Institute of Technology, Cambridge, MA 02139-4307, USA
[c] Department of Mechanical Engineering, Ben-Gurion University, 84105 Beer-Sheva, Israel
[d] Faculty of Aerospace Engineering, Israel Institute of Technology, Haifa 32000, Israel

ARTICLE INFO

Article history:
Received 14 December 2013
Received in revised form 1 April 2014
Available online 26 April 2014

Keywords:
Magnetorheological
Composites
Magnetostriction
Magnetoactive elastomers

ABSTRACT

We investigate the behavior of magnetoactive elastomers (MAEs) with periodic and random distributions of circular and elliptical fibers. For the MAEs with periodic microstructures, we develop finite element models and determine the local fields as well as the effective properties of MAEs with rectangular and quasi-hexagonal unit cells. For the MAEs with random microstructures, we derive a closed-form expression for the effective response making use of a recently developed theory (Ponte Castañeda and Galipeau, 2011). In particular, we determine the responses to pure shear loading in the presence of a magnetic field, both of which are aligned with the geometric axes of the fibers, and examine the roles of the deformation, concentration, particle shape, and distribution on the magnetostriction, actuation stress, and the magnetically induced stiffness of the composite. We show that the coupling effects are of second order in the concentration. This is consistent with the fact that these effects are primarily the result of the interaction between inclusions. We also demonstrate explicitly that the magnetomechanical coupling of these MAEs, when subjected to aligned loading conditions, depends not only on the magnetic susceptibility, but also, crucially, on its derivative with respect to the deformation. As a consequence, we find that the magnetoelastic effects may be quite different, even for composites with similar effective susceptibilities.

1. Introduction

Magnetoactive elastomers (MAEs) are composite materials exhibiting coupled magnetic and mechanical behavior. In this work we examine typical MAEs consisting of magnetically susceptible particles embedded in a non-magnetic soft elastomer matrix. Frequently used magnetic materials include carbonyl iron and nickel; examples of more exotic inclusions are Terfenol-D and Ni_2MnGa. MAEs are of interest because magnetic fields are capable of modifying the effective stiffness of the composite and of producing magnetostrictive strains. Both effects take place quickly and reversibly, making MAEs good candidates for tunable vibration dampers and magnetic actuators.

For MAEs made with inclusion materials such as carbonyl iron, nickel, or cobalt, which are effectively rigid compared to the elastomer matrix, the principal mechanisms are magnetic torques and magnetic interactions between particles (Jolly et al., 1996; Bednarek, 1999; Ginder et al., 2002; Guan et al., 2008). For the particular case when the magnetic particles are aligned with the external magnetic field, there are no magnetic torques on the particles and the magnetoelastic effects are controlled by particle interactions. Various approaches have been used to directly account for particle pair forces in MAEs in the context of infinitesimal deformations, including the works of Borcea and Bruno (2001), Yin and Sun (2006), and Yin et al. (2006).

Magnetic interactions in deformable elastic media can also be accounted for, in the context of a thermodynamically consistent formulation, by means of a free-energy function, leading to the notion of magnetic stresses, which exist even in vacuum (Maxwell, 1873). The pioneering works on electro- and magnetoelastic behavior of a continuum by Toupin (1956), Truesdell and Toupin (1960), Tiersten (1964), Brown (1966), and Maugin and Eringen (1972) have been recently reviewed and further developed by various authors (Brigadnov and Dorfmann, 2003; Dorfmann and Ogden, 2004a,b; Kankanala and Triantafyllidis, 2004; Vu and Steinmann, 2007; Bustamante et al., 2008). Making use of these constitutive formulations, Ponte Castañeda and Galipeau (2011) proposed a finite-strain, variational homogenization framework to determine the total magneto-elastic stress arising in a composite material as a consequence of combined magnetic and mechanical stimuli. Furthermore, for the special case of MAEs, where the magnetic particles are rigid compared to the soft elastomer matrix, Ponte Castañeda and Galipeau (2011) showed that the total stress

* Corresponding author. Tel.: +972 8 6477105; fax: +972 8 6477106.
E-mail address: debotton@bgu.ac.il (G. deBotton).

http://dx.doi.org/10.1016/j.ijsolstr.2014.04.013
0020-7683/

can be expressed as the sum of the purely mechanical stress, which exists in the composite when no magnetic fields are applied, together with the Maxwell stress in vacuum and an extra magnetic stress which is determined by the derivative of the (deformation-dependent) magnetic susceptibility of the composite with respect to the stretch. Applications of these results for MAEs with random microstructures and for magnetic fields that are aligned and unaligned with the anisotropic axes have been given by Galipeau and Ponte Castañeda (2012) and Galipeau and Ponte Castañeda (2013a), respectively. The mathematically analogous case of dielectric elastomer composites with periodic and random microstructures was considered by Ponte Castañeda and Siboni (2012) and Siboni and Ponte Castañeda (2013), respectively. In addition, deBotton et al. (2007) computed directly the macroscopic constitutive relations for electroelastic composites with layered microstructures, taking advantage of the fact that the fields are uniform in the layers. The stability of electroactive laminates was considered by Rudykh and deBotton (2011). The ability to significantly enhance the electromechanical coupling with appropriate arrangement of the microstructure of the composite was demonstrated in Tian et al. (2012) and Rudykh et al. (2013). Also, Galipeau and Ponte Castañeda (2013b) have recently shown that giant magnetostriction can be achieved in composites with herringbone-type microstructures by combining the action of magnetic torques with soft mechanical modes of deformation in the elastomer phase. Shear localization instabilities in layered and particulate magneto-elastic composites have been considered recently by Rudykh and Bertoldi (2013) and Galipeau and Ponte Castañeda (2013a), respectively. More general instabilities in the context of layered dielectric elastomers have been considered by Bertoldi and Gei (2011) and Rudykh et al. (2014).

Unfortunately, the set of microstructures for which exact analytical solutions can be obtained is essentially limited to materials with layered microstructures. For magneto-elastic materials with more general periodic microstructures, which have great potential for enhancing magneto-elastic performance, the exact behavior may be obtained by numerical computations. The finite element (FE) method is usually employed (Rudykh and deBotton, 2012) for this purpose. In this work, we pursue this approach for the coupled magnetomechanical problem and construct FE models for solving the magnetomechanical problem under finite deformations and periodic boundary conditions. Specifically, we examine periodic MAEs with (i) *rectangular* and (ii) *quasi-hexagonal* periodicity. The FE models provide the information about the local fields, which can be averaged over the unit cell to obtain the effective properties of the composites. For random microstructures, we estimate the effective behavior of MAEs with the homogenization-based constitutive model recently developed in Galipeau and Ponte Castañeda (2013a).

We define key parameters that govern the coupled magnetomechanical behavior of MAEs. These parameters are directly related to the applied traction measured on the surface of the material while accounting for the magnetic stresses outside the material. The governing parameters of the magnetomechanical coupling are evaluated for MAEs with random, quasi-hexagonal, and rectangular periodic microstructures over a wide range of concentrations and particle aspect ratios. We demonstrate explicitly that the magnetomechanical coupling depends not only on the magnetic susceptibility, but, more importantly, also on its derivative with respect to deformation. Accordingly, it is demonstrated that linearly magnetic materials with similar susceptibilities can exhibit rather different magneto-elastic coupling. Moreover, we find that, for some composites, while the magnetic induced tractions are larger, the magnetostriction is lower and vice versa. The two competing mechanisms that are responsible for this complex behavior are identified and discussed. Finally, in order to shed light on the complex dependence of the magneto-elastic coupling on the microstructure of the composite, we provide a qualitative analysis of this relation in terms of the magnetomechanical interactions among the inclusions.

In this work scalars will be denoted by italic Roman, a and G, or Greek letters, α and Γ; vectors by boldface Roman letters, $\mathbf{b}$; second-order tensors by boldface italic Roman letters, $\boldsymbol{P}$, or bold face Greek letters, $\boldsymbol{\epsilon}$. When necessary Cartesian components will be used; for example, P_{ij} are the Cartesian components of $\boldsymbol{P}$.

2. Magneto-elasticity in the quasistatic regime

Consider the quasistatic deformation of a body. In its reference configuration, the location of each material point is defined by the position vector $\mathbf{X}$. Under the combined action of mechanical and magnetic effects, the body deforms. In the deformed configuration, the new position of the material points is described by $\mathbf{x}$. The local deformation is characterized by the deformation gradient $\boldsymbol{F} = \operatorname{Grad}\mathbf{x}$, with Cartesian components $F_{ij} = \frac{\partial x_i}{\partial X_j}$, and is such that $J = \det \boldsymbol{F} > 0$. Conservation of mass implies that locally $\rho_0 = \rho J$, where ρ_0 and ρ are the material densities in the reference and deformed configurations, respectively. We also recall that the polar decomposition of the deformation gradient is $\boldsymbol{F} = \boldsymbol{RU}$, where $\boldsymbol{R}$ is the rotation and $\boldsymbol{U}$ is the stretch tensor.

We define $\boldsymbol{T}$ and $\boldsymbol{S} = J\boldsymbol{T}\boldsymbol{F}^{-T}$ to be the *total* Cauchy and (first) Piola–Kirchhoff stress tensors, respectively, which at static equilibrium and in the absence of body forces satisfy the equivalent mechanical equilibrium conditions

$$\operatorname{div}\boldsymbol{T} = 0 \quad \text{or} \quad \operatorname{Div}\boldsymbol{S} = 0. \tag{1}$$

The operators div and Div are the divergence operators with respect to $\mathbf{x}$ and $\mathbf{X}$, respectively. Together with the linear momentum balance Eq. (1), the stress fields also satisfy the balance of angular momentum. Accordingly, $\boldsymbol{T}^{\mathrm{T}} = \boldsymbol{T}$, or equivalently, $\boldsymbol{S}\boldsymbol{F}^{T} = \boldsymbol{F}\boldsymbol{S}^{T}$. The stress may be discontinuous across an interface, but must satisfy the jump conditions

$$[[\boldsymbol{T}]]\mathbf{n} = 0 \quad \text{or} \quad [[\boldsymbol{S}]]\mathbf{N} = 0, \tag{2}$$

where $\mathbf{n}$ and $\mathbf{N}$ denote the normal to the interface in the deformed and reference configurations, respectively.

The magnetic field is characterized by two primary magnetic field vectors: the magnetic induction $\mathbf{b}$ and the magnetic intensity $\mathbf{h}$, both defined in the current configuration. In the absence of surface charge and free currents, and for quasi-static conditions, they satisfy the field equations

$$\operatorname{div}\mathbf{b} = 0 \quad \text{and} \quad \operatorname{curl}\mathbf{h} = 0, \tag{3}$$

where the curl operator is with respect to $\mathbf{x}$. Alternatively, following the work of Dorfmann and Ogden (2004a), these equations can be written in Lagrangian form as

$$\operatorname{Div}\mathbf{B} = 0 \quad \text{and} \quad \operatorname{Curl}\mathbf{H} = 0, \tag{4}$$

where $\mathbf{B} = J\boldsymbol{F}^{-1}\mathbf{b}$ and $\mathbf{H} = \boldsymbol{F}^{T}\mathbf{h}$ are the Lagrangian counterparts of the magnetic fields and the Div and Curl operators are with respect to $\mathbf{X}$. The corresponding jump conditions at an interface are

$$[[\mathbf{b}]]\cdot\mathbf{n} = 0 \quad \text{and} \quad [[\mathbf{h}]]\times\mathbf{n} = 0, \tag{5}$$

or

$$[[\mathbf{B}]]\cdot\mathbf{N} = 0 \quad \text{and} \quad [[\mathbf{H}]]\times\mathbf{N} = 0. \tag{6}$$

The relation between the magnetic fields is customarily defined in terms of the magnetization $\mathbf{m}$, such that

$$\mathbf{h} = \frac{1}{\mu_0}\mathbf{b} - \mathbf{m}, \tag{7}$$

where μ_0 is the magnetic permeability of vacuum. In general, the magnetization depends on the material the body is made of, and is a function of the magnetic field and the deformation (Kovetz, 2000).

A thermodynamically consistent framework to describe magneto-elastic materials was developed by Brown (1966). More recently Kovetz (2000) made use of the method of Coleman and Noll (1963) to arrive at an equivalent formulation. Following these works we assume the existence of a free-energy function $\phi(\boldsymbol{F}, \mathbf{b})$. Thus, for quasi-static processes, the magnetic constitutive relation reduces to

$$\mathbf{m} = -\rho \frac{\partial \phi}{\partial \mathbf{b}} \tag{8}$$

and the total Cauchy stress is given by

$$\boldsymbol{T} = \rho \frac{\partial \phi}{\partial \boldsymbol{F}} \boldsymbol{F}^T - \frac{1}{2\mu_0}(\mathbf{b}\cdot\mathbf{b})\boldsymbol{I} + \frac{1}{\mu_0}\mathbf{b}\otimes\mathbf{b} + (\mathbf{m}\cdot\mathbf{b})\boldsymbol{I} - \mathbf{m}\otimes\mathbf{b}. \tag{9}$$

In terms of these relations, the energy–density function ϕ fully characterizes the behavior of the magneto-elastic material. Note that in the absence of a material, or when the material is non-magnetic, there still exists a stress tensor which depends on the magnetic field, also referred to as the Maxwell stress. A Lagrangian "amended" free energy function can be constructed, in terms of ϕ, as (Dorfmann and Ogden, 2004a)

$$W(\boldsymbol{F}, \mathbf{B}) = \rho_0 \phi\left(\boldsymbol{F}, \frac{1}{J}\boldsymbol{F}\mathbf{B}\right) + \frac{\boldsymbol{F}\mathbf{B}\cdot\boldsymbol{F}\mathbf{B}}{2\mu_0 J}. \tag{10}$$

Then, the conjugate Lagrangian variables are given by

$$\mathbf{H} = \frac{\partial W}{\partial \mathbf{B}} \quad \text{and} \quad \boldsymbol{S} = \frac{\partial W}{\partial \boldsymbol{F}}. \tag{11}$$

For incompressible materials the deformation is constrained so that

$$\det \boldsymbol{F} = 1. \tag{12}$$

The corresponding total stress is

$$\boldsymbol{T} = \frac{\partial W}{\partial \boldsymbol{F}} \boldsymbol{F}^{\mathrm{T}} - p\boldsymbol{I}, \tag{13}$$

where p is a Lagrange multiplier associated with the incompressibility constraint.

Motivated by experimental studies of MAEs (Jolly et al., 1996; Bednarek, 1999; Ginder et al., 2002; Guan et al., 2008; Danas et al., 2012), where the sample is subjected to combined magnetic field and applied *traction*, we establish the relation between the applied traction and the total stress within the material. We recall that the magnetic fields extend past the body into its surrounding (vacuum or non-magnetic material), and that these magnetic fields generate Maxwell stresses outside the body. Based on the jump conditions (5), the magnetic fields and subsequently the magnetic stress outside the material can be determined from the magnetic fields inside the material. Consequently, it can be shown that the traction on the boundary of the specimen is (Kankanala and Triantafyllidis, 2004)

$$\mathbf{t} = \left[\boldsymbol{T} + \left(\frac{\mu_0}{2}(\mathbf{h}\cdot\mathbf{h})\boldsymbol{I} - \mathbf{h}\otimes\mathbf{b}\right)\right]\mathbf{n} - \frac{\mu_0}{2}(\mathbf{m}\cdot\mathbf{n})^2\mathbf{n}, \tag{14}$$

where $\boldsymbol{T}$, $\mathbf{h}$, $\mathbf{b}$, and $\mathbf{m}$ are the fields (in the material) just inside the boundary and $\mathbf{n}$ is the outward normal to the boundary. Although this formula is written in terms of $\boldsymbol{T}$, $\mathbf{h}$, $\mathbf{b}$ and $\mathbf{m}$ for convenience, these are not all independent variables. For instance, once $\mathbf{b}$ and $\boldsymbol{F}$ are specified, they determine all other variables via the constitutive relations of the material. In addition, note that, in the absence of a magnetic field, the above expression reduces to its usual form in the purely mechanical case, i.e., $\mathbf{t} = \boldsymbol{T}\mathbf{n}$. When a non-magnetic material is being tested, the magnetic stresses are self-equilibrated and magnetic fields have no effect on the traction.

When two or more magneto-elastic materials are combined together in such a way that the size of the sample is significantly larger than the characteristic size of the microstructure, the material is said to satisfy the separation of length scale hypothesis and the material forms a composite. Moreover, if the variation of the applied boundary condition are larger than the characteristic size of the heterogeneity, the composite can be treated as a homogenous material with effective constitutive properties. Roughly speaking, these effective properties characterize the relationship between the volume averaged field quantities within a representative volume element of the material (Ponte Castañeda and Galipeau, 2011).

The representative volume element can be identified with Ω_0 which, due to the magnetomechanical loading, transforms into a new region Ω. Volume average field quantities are denoted with over-bar. Lagrangian fields such as $\boldsymbol{F}$, $\boldsymbol{S}$, $\mathbf{B}$, and $\mathbf{H}$ are averaged over the reference region Ω_0. For example,

$$\bar{\boldsymbol{F}} = \frac{1}{|\Omega_0|}\int_{\Omega_0} \boldsymbol{F} dV. \tag{15}$$

Eulerian fields like $\boldsymbol{T}$, $\mathbf{b}$, $\mathbf{h}$, and $\mathbf{m}$, are averaged over the deformed configuration. For example,

$$\bar{\boldsymbol{T}} = \frac{1}{|\Omega|}\int_{\Omega} \boldsymbol{T} d\upsilon. \tag{16}$$

In the above expressions $|\Omega_0|$ and $|\Omega|$ denote the volumes of the undeformed and the deformed regions, respectively.

Additionally, when the behaviors of the phases are characterized by energy–density functions, the overall behavior of the composite can be characterized by a homogenized energy–density function $\tilde{W}(\bar{\boldsymbol{F}}, \bar{\mathbf{B}})$ or, alternatively, $\tilde{\phi}(\bar{\boldsymbol{F}}, \bar{\mathbf{b}})$. The Lagrangian energy function $\tilde{W}(\bar{\boldsymbol{F}}, \bar{\mathbf{B}})$ is determined by averaging the local energy over the reference configuration consistent with the homogenization approach of Ponte Castañeda and Galipeau (2011). This Lagrangian energy–density is used to define the corresponding Eulerian energy–density function via Eq. (10).

In this work we consider the effective behavior of MAEs with random and periodic distributions of magnetoactive particles in a soft matrix. For composites with random distributions, the homogenization is performed by considering the response of a representative volume element in which the microstructure is not specified exactly and the effective energy–density function depends on available two-point statistical information.

For periodic media the microstructure is fully determined once the unit cell is specified. The effective properties can be found by evaluating the response of the primitive unit cell under periodic boundary conditions. Once again, we assume that the material occupies a sufficiently large domain and the influence of the boundary effects can be neglected. This applies up to the onset of instabilities at which the periodicity scale can spontaneously change and become larger than the single unit cell (Geymonat et al., 1993). These effects are beyond the scope of this work and we restrict our study to the "principal" solutions along the prescribed loading paths.

3. Analysis of MAE composites with aligned fibers

We consider orthotropic MAE composites with long cylindrical rigid fibers aligned along the $\hat{\mathbf{e}}_3$-axis. The fibers, with elliptic cross-section, are distributed such that their principal axes are aligned with the $\hat{\mathbf{e}}_1$ and $\hat{\mathbf{e}}_2$ axes. We assume that the composites are incompressible, and determine their response to a 2-D magnetomechanical loading consistent with the pure shear deformation

$$\bar{\boldsymbol{F}} = \bar{\lambda}\hat{\mathbf{e}}_1 \otimes \hat{\mathbf{e}}_1 + \bar{\lambda}^{-1}\hat{\mathbf{e}}_2 \otimes \hat{\mathbf{e}}_2 \tag{17}$$

and the mean magnetic field

$$\bar{\mathbf{b}} = \bar{b}\,\hat{\mathbf{e}}_1. \tag{18}$$

The loading plane, which is transverse to the long axis of the fibers, is schematically shown in Fig. 1. Under these loading conditions, the stress tensor $\boldsymbol{T}$ has components along both axes. However, by eliminating the Lagrange multiplier associated with the incompressibility constraint, we can define the deviatoric stress component

$$\bar{T} = \bar{T}_{11} - \bar{T}_{22}. \tag{19}$$

This implies that only one mechanical traction component, say $\bar{t}$ along $\hat{\mathbf{e}}_1$, is needed to attain the specified deformation. Alternatively, $\bar{t}$ may represent the difference between the normal tractions on the surfaces perpendicular to the axes. Note that these loading conditions will result in a uniaxial motion of the specimen as in a "linear actuator."

In connection with Fig. 1, it is important to emphasize that the diagram is *not* meant to suggest that the response of any given specimen is independent of its overall shape. Indeed, in general, it is not possible to generate uniform fields inside a specimen of an arbitrary shape when it is subjected to a uniform, remotely applied, magnetic field. This is due to the so-called demagnetizing fields. Typically, it is necessary to either use very long, or very short cylindrical specimens, with the fields applied along the axis of the cylinder. In such cases, the magnetic fields generated in homogeneous specimens are nearly uniform, except at the corners and the edges of the specimen where fringe fields are generated. In this work, we are interested in describing the macroscopic (material) response of the MAEs and for this reason we will not worry about how such uniform fields may be generated, and assume simply that this can be done, at least approximately. In addition, by using the fields *inside* the specimen to describe the response, we also avoid the difficulties associated with relating the remotely applied fields to the actual fields generated inside the specimen. Clearly, this more difficult problem can also be handled using the homogenized properties of the MAE in the context of a suitably defined boundary value problem to be solved numerically, but, again, this is beyond the scope of this work.

In view of the alignment of the loading with the orthotropic axes of the MAE (as determined by the aligned fibers), it can be assumed that the fibers do not rotate with respect to the magnetic field, and the material symmetry remains unchanged under all magneto-elastic loading conditions. This condition holds true for periodic composites up to the onset of bifurcations, and should remain a good assumption for MAEs with random microstructures. These conditions imply that the composite will exhibit a linear relationship between $\bar{b}, \bar{h}$ and $\bar{m}$, since the matrix and the particle have linear magnetization relations. Consequently, the macroscopic magnetic relations for the composite can be written as

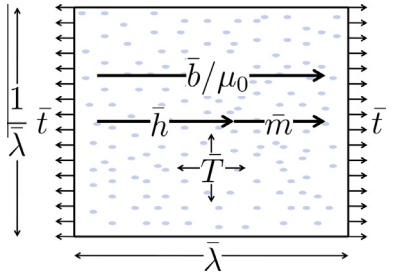

Fig. 1. A sketch of the MAE sample and the magnetomechanical boundary conditions.

$$\bar{m} = \tilde{\chi}(\bar{\lambda})\frac{\bar{b}}{\mu_0} \quad \text{or} \quad \bar{h} = \left[1 - \tilde{\chi}(\bar{\lambda})\right]\frac{\bar{b}}{\mu_0}, \tag{20}$$

where $\bar{m}$ is the magnetization and $\tilde{\chi}(\bar{\lambda})$ is the effective magnetic susceptibility of the composite which is a function of the macroscopic stretch.

Using Eq. (8), the effective energy–density for these composites under these loading conditions may be obtained as

$$\tilde{\phi}(\bar{\lambda}, \bar{b}) = \tilde{\phi}_{\mathrm{me}}(\bar{\lambda}) - \tilde{\chi}(\bar{\lambda})\frac{\bar{b}^2}{2\bar{\rho}\mu_0}, \tag{21}$$

where $\tilde{\phi}_{\mathrm{me}}(\bar{\lambda})$ is a function of the stretch only. Note that if $\bar{b} = 0$, $\tilde{\phi}_{\mathrm{me}}(\bar{\lambda})$ is essentially the effective mechanical energy–density function of the composite in the absence of a magnetic field. Note also that the expression for the aligned loadings (21) is a special case of a more general result (see Eq. (85) in Ponte Castañeda and Galipeau (2011)).

From Eq. (21), together with the incompressibility assumption and Eqs. (13), (17), (18) and (19), the overall stress in the composite is given by

$$\bar{T} = \bar{T}_{me}(\bar{\lambda}) + \frac{\mu_0}{2}\,\bar{\lambda}\bar{m}^2\,\frac{\partial\tilde{\chi}^{-1}(\bar{\lambda})}{\partial\bar{\lambda}} + \frac{\bar{b}^2}{\mu_0} - \bar{m}\bar{b}, \tag{22}$$

where

$$\bar{T}_{me}(\bar{\lambda}) = \bar{\rho}\,\bar{\lambda}\,\frac{\partial\tilde{\phi}_{\mathrm{me}}(\bar{\lambda})}{\partial\bar{\lambda}} \tag{23}$$

is the "mechanical" stress. Additionally, accounting for the boundary effects of the magnetic field via Eq. (14), the associated applied traction is

$$\bar{t} = \bar{T}_{me}(\bar{\lambda}) + \mu_0\bar{m}^2\,\tilde{\Upsilon}(\bar{\lambda}) \equiv \bar{t}(\bar{\lambda}, \bar{b}), \tag{24}$$

where the *magneto-elastic coupling coefficient* is

$$\tilde{\Upsilon}(\bar{\lambda}) \equiv \frac{\bar{\lambda}}{2}\frac{\partial\tilde{\chi}^{-1}(\bar{\lambda})}{\partial\bar{\lambda}} - \frac{1}{2}. \tag{25}$$

We note that the magneto-elastic coupling in expression (24) is related to the derivative of the susceptibility $\tilde{\chi}$ and is quadratic in the magnetization (which, by $(20)_1$ also depends on $\tilde{\chi}$). In particular, the magneto-elastic coupling coefficient can be directly related to the actuation traction and the magnetostriction. The actuation traction $\bar{t}_a$ is defined as the traction when no macroscopic deformation is applied, that is the traction developing due to the magnetic field while the material is held in its referential configuration. Since the mechanical stress vanishes when $\bar{\lambda} = 1$, the actuation traction is purely magnetic and is given by

$$\bar{t}_a \equiv \bar{t}(1, \bar{b}) = \frac{1}{\mu_0}\left[\tilde{\chi}(1)\right]^2\tilde{\Upsilon}(1)\,\bar{b}^2, \tag{26}$$

where use has been made of Eq. $(20)_1$. Analogously, magnetostriction is the stretch that develops in the material when subjected to vanishing mechanical tractions on the boundary of the specimen. The magnetostrictive stretch $\bar{\lambda}_{\mathrm{m}}$ is thus determined by solving the equation

$$-\bar{T}_{me}(\bar{\lambda}_{\mathrm{m}}) = \frac{1}{\mu_0}\left[\tilde{\chi}(\bar{\lambda}_m)\right]^2\tilde{\Upsilon}(\bar{\lambda}_{\mathrm{m}})\,\bar{b}^2, \tag{27}$$

where once again we have made use of Eq. $(20)_1$ for $\bar{m}$. Note that $\bar{\lambda}_{\mathrm{m}}$ is a function of the applied magnetic induction $\bar{b}$.

Furthermore, the magneto-elastic coupling coefficient determines how the magnetic field changes the effective stiffness. Specifically, we define the effective tangent Young's modulus as the derivative of the traction with respect to the logarithmic strain $\bar{e} = \ln\bar{\lambda}$. That is

$$\tilde{E} \equiv \frac{\partial \bar{t}}{\partial \bar{e}}. \tag{28}$$

From Eq. (24), we find that

$$\tilde{E} = \tilde{E}_{me}(\bar{\lambda}) + \mu_0 \bar{m}^2 \bar{\lambda} \frac{\partial \tilde{\Upsilon}(\bar{\lambda})}{\partial \bar{\lambda}} + 2\mu_0 \bar{m} \bar{\lambda} \tilde{\Upsilon}(\bar{\lambda}) \frac{\partial \bar{m}}{\partial \bar{\lambda}}, \tag{29}$$

where $\tilde{E}_{me}(\bar{\lambda}) \equiv \bar{\lambda} \frac{\partial \bar{T}_{me}(\bar{\lambda})}{\partial \bar{\lambda}}$ is the purely mechanical Young's modulus, which, as it should, reduces to the linear Young's modulus of the composite in the infinitesimal strain limit. We note that $\tilde{E}$ depends on both the mechanical and magnetic loading conditions. Here, for convenience, we examine its dependence on the deformation when the magnetization $\bar{m}$ is held fixed with respect to the deformation. (This would be the case, for example, for ferromagnetic particles at saturation.) In this case the *magnetic tangent Young's modulus* is

$$\tilde{E}_{mag}(\bar{\lambda}) \equiv \mu_0 \bar{m}^2 \bar{\lambda} \frac{\partial \tilde{\Upsilon}(\bar{\lambda})}{\partial \bar{\lambda}} = \mu_0 \bar{m}^2 \frac{\bar{\lambda}}{2} \left(\bar{\lambda} \frac{\partial^2 \tilde{\chi}^{-1}(\bar{\lambda})}{\partial \bar{\lambda}^2} + \frac{\partial \tilde{\chi}^{-1}(\bar{\lambda})}{\partial \bar{\lambda}} \right). \tag{30}$$

Note that the sign of $\tilde{E}_{mag}$ determines whether the magnetic field stiffens or softens the composite in the loading direction. Clearly, since $\bar{\lambda}, \bar{m}^2$, and μ_0 can take only positive values, the sign of $\tilde{E}_{mag}$ is determined by the sign of $\frac{\partial \tilde{\Upsilon}(\bar{\lambda})}{\partial \bar{\lambda}}$.

Consistent with the general findings of Ponte Castañeda and Galipeau (2011), Eqs. (24)–(30) suggest that the magneto-elastic coupling properties of the composite depend not only on the susceptibility $\tilde{\chi}$, but more importantly also on its derivatives with respect to the deformation. Moreover, MAEs with different microstructures may be characterized by the same macroscopic magnetic response, while still having significantly different magnetomechanical response (see also Tian et al., 2012, in the context of dielectric composites). Interestingly, the coupled magnetomechanical behavior of MAEs with the same constituents and similar volume fractions may be significantly different. Moreover, the magnetic field may either stiffen or soften the composites depending on their microstructure. To highlight these effects, in the following sections we compare the behaviors of MAE composites with several different microstructures.

To complete the discussion, we note that there are two competing mechanisms associated with increases in the concentration of the stiff, magnetic inclusions in the MAE composites. On the one hand, when the concentration is increased, the magnetic forces developed in the composite increase; however, on the other, the composite's overall mechanical stiffness also increases. As a result the magnetostriction and the sensitivity of the composite to the magnetic field may increase or decrease depending on the relative contributions of these two effects. The first effect is essentially captured by the magneto-elastic coupling coefficient $\tilde{\Upsilon}$. To examine the second effect, we recall that for composites with rigid inclusions the primary parameters controlling the overall mechanical stiffness are the elastomer matrix stiffness, which in the limit of small strains is characterized by the shear modulus $G_0^{(1)}$, and the volume fraction of the inclusions c. (Here and henceforth the superscript (1) will be used to label the matrix phase.) Accordingly, we define the "mechanical stress concentration" $\tilde{N}$, such that

$$\bar{T}_{me} = T_{me}^{(1)}(\bar{\lambda}) + \tilde{N} G_0^{(1)} c \ln(\bar{\lambda}), \tag{31}$$

where $T_{me}^{(1)} = \frac{\partial \phi^{(1)}}{\partial \lambda}$ is the mechanical stress in the homogenous matrix material when subjected to the deformation described in Eq. (17). Note that $\tilde{N}$ does not vanish at zero volume fraction, nor at zero strain.

4. Macroscopic response of MAEs with different microstructures

Recalling that the typical elastomer matrix phase is non-magnetic, we assume that its behavior can be described by a purely mechanical neo-Hookean model. Accordingly, the matrix energy–density function is

$$\phi^{(1)}(\boldsymbol{F}) = \frac{G_0^{(1)}}{2\rho_0^{(1)}} \left[\mathrm{tr}(\boldsymbol{F}^{\mathrm{T}}\boldsymbol{F}) - 2 \right]. \tag{32}$$

The total stress tensor in the matrix phase, which is given in expression (9), includes the magnetic Maxwell stress and, consequently, depends on the local magnetic field as well.

In accordance with the assumed linear magnetic behavior of the fibers, their response is characterized by

$$\phi^{(2)}(\boldsymbol{F}, \mathbf{b}) = \phi_{\mathrm{me}}^{(2)}(\boldsymbol{F}) - \frac{\chi}{2\rho^{(2)}\mu_0} \mathbf{b} \cdot \mathbf{b}, \tag{33}$$

where χ is the magnetic susceptibility, and the superscript (2) denotes the inclusion phase. The rigidity of the particles is enforced by assuming that $\phi_{\mathrm{me}}^{(2)}(\boldsymbol{F})$ is equal to zero, if $\boldsymbol{F}$ is a pure rotation, and infinity otherwise.

As described previously, these two phases can be arranged in different ways to generate composites with aligned, cylindrical fibers of elliptical cross section exhibiting different magneto-elastic properties. In this work we examine the responses of MAEs with three different microstructures: (i) MAEs with *random* distributions of the aligned, elliptical, magnetoactive particles (Fig. 2); (ii) MAEs with *periodic rectangular* distribution (Fig. 3(a)); (iii) MAEs with *periodic quasi-hexagonal* distribution (Fig. 3(b)).

The effective energy–density function of the MAEs with the random microstructure is characterized by the concentration c, the aspect ratio w of the fibers cross-section, and their distribution. The particles are assumed to be distributed randomly with "elliptical" symmetry characterizing the average distance between the particles in different directions (Ponte Castañeda and Willis, 1995). In this work we assume an initial elliptical distribution with an aspect ratio identical to the fiber cross-section.

Specializing the work of Lopez-Pamies and Ponte Castañeda (2006a) and Lopez-Pamies and Ponte Castañeda (2006b) to uniaxial loading along the fiber direction, the homogenized mechanical energy is

$$\tilde{\phi}_{\mathrm{me}}^{(\mathrm{ran})}(\bar{\lambda}) = \frac{G}{2\bar{\rho}_0}(1-c) \left(\frac{\left(1+2(c-2)c\bar{\lambda}^2+\bar{\lambda}^4\right)w + c\left(1-\bar{\lambda}^4\right)\left(1+w^2\right)}{(1-c)^2\bar{\lambda}^2 w} - 2 \right). \tag{34}$$

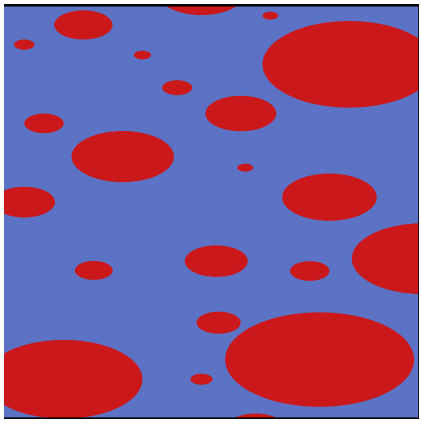

Fig. 2. A schematic representation of MAE composite with random distribution of magnetoactive particles in a soft matrix.

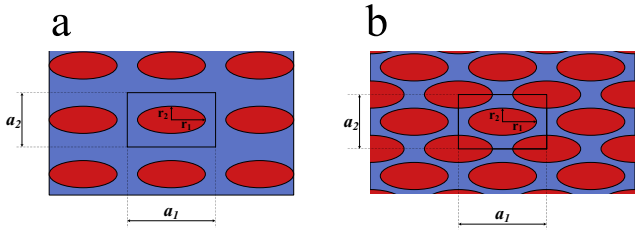

Fig. 3. A schematic representation of MAE composites with (a) a rectangular and (b) an hexagonal periodic distributions of magnetoactive particles in a soft matrix.

Similarly, specializing Galipeau and Ponte Castañeda (2013a) to uniaxial loading along the fiber direction, we write the effective susceptibility $\tilde{\chi}(\bar{\lambda})$ for the aligned loading in the form

$$\tilde{\chi}^{(\mathrm{ran})}(\bar{\lambda}) = c\left[\frac{1}{\chi} - \frac{w}{w+1} + c\frac{w\bar{\lambda}^2}{w\bar{\lambda}^2+1}\right]^{-1}. \tag{35}$$

Note that $w\bar{\lambda}^2$ represents the aspect ratio of the distributional ellipsoid in the deformed configuration.

From expressions (35) and (25), the magneto-elastic coupling coefficient can then be determined explicitly as

$$\tilde{\Upsilon}^{(\mathrm{ran})}(\bar{\lambda}) = \frac{w\bar{\lambda}^2}{\left(1+w\bar{\lambda}^2\right)^2} - \frac{1}{2}, \tag{36}$$

while the effective elastic modulus is obtained from Eq. (30) as

$$\frac{\tilde{E}_{mag}}{\mu_0\bar{m}^2} = \frac{2w\bar{\lambda}^2\left(1-w\bar{\lambda}^2\right)}{\left(1+w\bar{\lambda}^2\right)^3}. \tag{37}$$

To analyze the behaviors of MAEs with periodic microstructures, we use a finite element (FE) model. We examine periodic MAEs with two unit cells, rectangular and quasi-hexagonal (see Fig. 3). The precise details of the cells can be varied by changing the aspect ratio of the unit cell, the aspect ratio of the inclusion, and the inclusion concentration.

To prevent the particles from extending past the unit cell and to maintain geometric similarity with the random microstructures, the aspect ratio of the unit cells is identified with the aspect ratio of the particles. Thus, for the rectangular unit cells, the ratio between the lengths of the vertical and horizontal faces (a_1 and a_2, respectively) varies with the inclusion aspect ratio such that

$$a_1^{(rec)}/a_2^{(rec)} = w, \tag{38}$$

while for the hexagonal unit cell the ratio between the lengths of vertical and horizontal sides is given by

$$a_1^{(hex)}/a_2^{(hex)} = \sqrt{3}w. \tag{39}$$

For convenience, we set the origin of the coordinate system at the center of one of the particles. Accordingly, in the reference configuration Ω_0, the domain of the unit cell is

$$-\frac{a_1}{2} \leqslant X_1 \leqslant \frac{a_1}{2}, \quad -\frac{a_2}{2} \leqslant X_2 \leqslant \frac{a_2}{2}. \tag{40}$$

The radii of the inclusions are defined according to the inclusion volume fraction and the geometry of the unit cell. Thus, for the two distributions,

$$r_2^{(rec)} = \left(\frac{c}{\pi}\right)^{1/2} a_2 \quad \text{and} \quad r_2^{(hex)} = \left(\frac{\sqrt{3}c}{2\pi}\right)^{1/2} a_2 \tag{41}$$

and $r_1 = wr_2$.

The magnetomechanical loading is implemented by applying periodic boundary conditions for both the displacement and the magnetic field (see Michel et al., 2010, 2012, in the mechanical context). This is accomplished by specifying the stretch $\bar{\lambda}$ and the magnetostatic potential φ on the boundary of the composite. (Since Curl $\mathbf{H} = 0$, there exists a scalar field, the magnetostatic potential φ, such that $\mathbf{H} = -\mathrm{Grad}\,\varphi$.) At the top $\left(X_2 = \frac{a_2}{2}\right)$ and the bottom $\left(X_2 = -\frac{a_2}{2}\right)$ faces of the unit cell the deformation and the magnetostatic potential are

$$\begin{cases} x_1^{(T)} = x_1^{(B)} \\ x_2^{(T)} = x_2^{(B)} + \frac{1}{\lambda}a \\ \varphi^{(T)} = \varphi^{(B)} \end{cases}. \tag{42}$$

At the right $\left(X_1 = \frac{a_1}{2}\right)$ and the left $\left(X_1 = -\frac{a_1}{2}\right)$ faces the deformation and the magnetostatic potential are

$$\begin{cases} x_1^{(L)} = x_1^{(R)} + \bar{\lambda}b \\ x_2^{(L)} = x_2^{(R)} \\ \varphi^{(L)} = \varphi^{(R)} + \bar{H}b \end{cases}. \tag{43}$$

Note that for the FE solution we use the magnetic intensity $\mathbf{H}$ as the independent variable. The boundary value problems are solved with the commercial FE code COMSOL Multiphysics. Once the local fields are determined, the effective response is calculated by suitably averaging the local fields over the relevant domain.

For the purposes of the FE simulations, the shear modulus of the matrix is set to $G_0^{(1)} = 1$ MPa. Since the fibers must be "deformable" for the FE simulations, their mechanical behavior is taken to be identical to that of the matrix, but with an initial shear modulus $G_0^{(2)} = 1$ GPa. This is consistent with the fact that the inclusions are stiff and the matrix accommodates the deformation. In general, the FE simulation would need to be performed for each combination of $\bar{\lambda}$ and $\bar{H}$. However, for each value of $\bar{\lambda}$, we can perform the FE simulations at $\bar{H} = 0$ and a non-zero $\bar{H}$, and extrapolate to all other values of the magnetic field based on the analysis in Section 3. Here we take the nonzero value of

$$\bar{H} = \sqrt{\frac{G_0^{(1)}}{\mu_0}}, \tag{44}$$

so that the magnitude of the magneto-elastic stresses is comparable with that of the purely mechanical stresses.

From the data obtained for $\bar{\mathbf{B}}$, $\bar{\mathbf{H}}$, $\bar{\boldsymbol{F}}$, $\bar{\mathbf{T}}$ and $\bar{\mathbf{T}}_{\mathrm{me}}$ as functions of $\bar{\lambda}$, the corresponding scalars $\bar{b}$, $\bar{h}$, $\bar{m}$, $\bar{T}$, $\bar{T}_{\mathrm{me}}$ and the magneto-elastic coupling coefficient $\tilde{\Upsilon}$ are computed. In this regard, we note that there are two ways to determine $\tilde{\Upsilon}$ from the quantities extracted from the FE simulation. The first is from Eq. (22) for the total stress $\bar{T}$ in terms of $\bar{b}$, $\bar{h}$, $\bar{m}$, $\bar{\lambda}$, and $\bar{T}_{\mathrm{me}}$, leading to

$$\tilde{\Upsilon}^{(\mathrm{T})}(\bar{\lambda}) = \frac{\bar{T} - \left(\bar{T}_{\mathrm{me}} + \bar{b}^2/\mu_0 - \bar{m}\bar{b}\right)}{\mu_0\bar{m}^2} - \frac{1}{2}. \tag{45}$$

The second is to determine the susceptibility $\tilde{\chi}$ from Eq. (20) in terms of $\bar{b}$ and $\bar{m}$, and to compute incremental changes in this quantity as a function of $\bar{\lambda}$. According to this procedure, we have that

$$\tilde{\Upsilon}^{(\chi)}(\bar{\lambda}) = \frac{1}{\mu_0}\frac{\partial(\bar{b}/\bar{m})}{\partial\bar{\lambda}}\frac{\bar{\lambda}}{2} - \frac{1}{2}. \tag{46}$$

Assuming that the FE simulations are sufficiently accurate, these two procedures should lead to identical results (i.e., $\tilde{\Upsilon}^{(\mathrm{T})} = \tilde{\Upsilon}^{(\chi)}$). Indeed, this was the case for the results shown in the next section, thus providing a valuable internal check on the accuracy of the numerical simulations, as well as on the validity of formula (25) for the magneto-elastic coupling coefficient $\tilde{\Upsilon}$.

5. Results and discussion

To highlight and compare the coupled magneto-elastic behaviors of the different microstructures, we systematically analyze

the variations of the following four parameters as functions of the deformation:

(a) The effective susceptibility normalized by the fiber concentration $\tilde{\chi}/c$, a quantity describing the magnetization of the composite.
(b) The mechanical stress concentration $\tilde{N}$ due to the presence of the fibers. This is a measure of the purely mechanical reinforcement of the composite relative to the elastomer matrix.
(c) The magneto-elastic coupling coefficient $\tilde{\Upsilon}$ providing information about the magnetic contribution to the stresses in the composite.
(d) The normalized magnetic tangent Young's modulus $\tilde{E}_{mag}(\bar{\lambda})/(\mu_0\bar{m}^2)$. This quantity captures the contribution of the magnetic field to the overall stiffness of the composite.

For conciseness, in the following we refer to a composite with a random distribution of the fibers as a "random composite". Similarly, we denote "hexagonal composite" and "rectangular composite" periodic composites with hexagonal and rectangular distributions of the fibers, respectively.

We begin by examining the variations of the four, above-described parameters as functions of the stretch $\bar{\lambda}$. Fig. 4 displays their variations for composites with aspect ratio $w = 1$ and volume fraction $c = 0.1$, as functions of the logarithmic strain $\bar{e} = \ln\bar{\lambda}$. As the composite is compressed ($\bar{\lambda} < 1$; see Fig. 4(a)), the particles get closer in the direction of the magnetic field and the susceptibility increases as shown in Fig. 4(a). This is consistent with the anticipated enhancement of the magnetic interactions between the particles. The mechanical reinforcement in these three composites is quite similar in the reference configuration but varies rather differently at large stretch ratios as shown in Fig. 4(b). The fact that $\tilde{N}$ changes with the deformation demonstrates the nonlinearity of the mechanical reinforcement as a function of the strain. Obviously, this nonlinearity must be accounted for when considering large magnetostriction.

Remarkably, as shown in Fig. 4c, these materials exhibit very different magneto-elastic coupling. The magneto-elastic coupling coefficient $\tilde{\Upsilon}$ can be either positive or negative. Accordingly, the magnetostriction may lead to extension or compression in the direction of the applied field. For the random composite, this coefficient is fairly independent of the stretch, while for the periodic microstructures it changes significantly. Moreover, for the hexagonal composite $\tilde{\Upsilon}$ may change its sign depending on the stretch.

Fig. 4(d), depicting the variations in the magnetic tangent Young's modulus, reinforces these observations. Thus, for random composites the dependence of $\tilde{E}_{mag}$ on the deformation is weak. For the rectangular composites, this modulus is close to zero in the undeformed state ($\bar{e} = 0$), but becomes negative or positive depending on whether the composite is subjected to compression or tension, respectively. The picture is more complicated with regard to the hexagonal composite where the magnetic field softens the composites even at the undeformed configuration. This effect is preserved under compressive loads. However, when the material is subjected to tension, there is an increase in $\tilde{E}_{mag}$ up to a certain level of the stretch at which the modulus becomes positive. This implies that from this point on the magnetic field stiffens the composite. The variabilities in these effects with respect to the deformation demonstrate the sensitivity of magneto-elastic coupling to the microstructure. At the end of this section, we qualitatively analyze these phenomena and provide further insight into the mechanisms responsible for these differences.

Fig. 5 shows the variations of the four parameters as functions of the stretch for composites with particle aspect ratios $w = 1/4$ and $w = 4$. Note that some of the curves were terminated when the FE model failed to converge. The effective susceptibilities of the composites are strongly dependent on the particle shape. In particular, as shown in Fig. 5(a), the susceptibility of the composites with particles elongated in the direction of the magnetic field ($w = 4$) is larger than that of the composites with $w = 1/4$. The difference is due to the fact that the particles are more strongly magnetized when their long axis is aligned with the applied field. Additionally, the susceptibilities of composites with $w = 4$ depend on the deformation more strongly than for composites with $w = 1/4$.

The aspect ratio clearly also affects the mechanical response of the composite as can be deduced from Fig. 5(b). However, this effect is rather different in MAEs with random and periodic distributions of the particles. Whereas the mechanical reinforcement is the same for both aspect ratios for random composites, the periodic composites with $w = 4$ and $w = 1/4$ exhibit rather different mechanical responses. These effects are important because while some microstructures result in stronger magnetic effects, the mechanical interactions between the inclusions in these materials may be stronger too, thus leading to a stiffer mechanical response and diminishing the overall magnetomechanical coupling.

Fig. 5(c) shows the corresponding dependence of the magneto-elastic coupling coefficient. Once again, for the random composites, the effect of the deformation is small and almost independent of the deformation. For the periodic composites, on the other hand, the change is more pronounced in terms of both the magnitude and the slope. For $w = 4$ the positive slopes indicate that the level of the magnetically induced stresses in the periodic composites increase with $\bar{\lambda}$, while the negative slopes for $w = 1/4$ indicate the opposite trend. These observations are in agreement with the curves shown in Fig. 5(d). There are negligible variations in the magnetic part of the stiffness for the random composites, positive contribution to the stiffness of the periodic composites with $w = 4$, and negative for the oblate periodic composites.

Next, we consider the influence of the inclusions volume fraction. Thus, Fig. 6 shows the variations of the four parameters as functions of c. We note that in the small concentration limit ($c \ll 1$) the mechanical stress concentration and magnetic susceptibility exhibit similar trends for composites with similar aspect ratios. This observation is consistent with the result of Eshelby (1957) for composites with dilute inclusion concentration. Indeed, the results of Ponte Castañeda and Willis (1995) show that in the dilute limit the macroscopic response of the composite depends only on the particle shape and not on the distribution shape. However, the coupled magneto-elastic properties of these composites behave differently in this limit. To highlight the physics responsible for this effect, consider the expansion of the susceptibility for small concentrations

$$\tilde{\chi} = \tilde{\chi}_0 c + \tilde{\chi}_1 c^2 + o(c^3). \tag{47}$$

The dilute result for particulate composites guarantees that $\tilde{\chi}_0$ only depends on the shape of the particle so that this term is the same for each microstructure if w is the same; specifically,

$$\tilde{\chi}_0 = \frac{\chi(w+1)}{1+w(1-\chi)}. \tag{48}$$

Therefore, for the composites considered in this work, $\tilde{\chi}_0$ is independent of deformation because the rigid fibers do not change their shape, and their volume fractions does not change due to incompressibility. Thus, the magnetomechanical coupling parameter and magneto-elastic modulus are determined to leading order by $\tilde{\chi}_1$. This is consistent with the fact that $\tilde{\chi}_1$ depends on the interactions between the particles and hence on their relative positions, as specified by the particle distribution, and is therefore different for different microstructures.

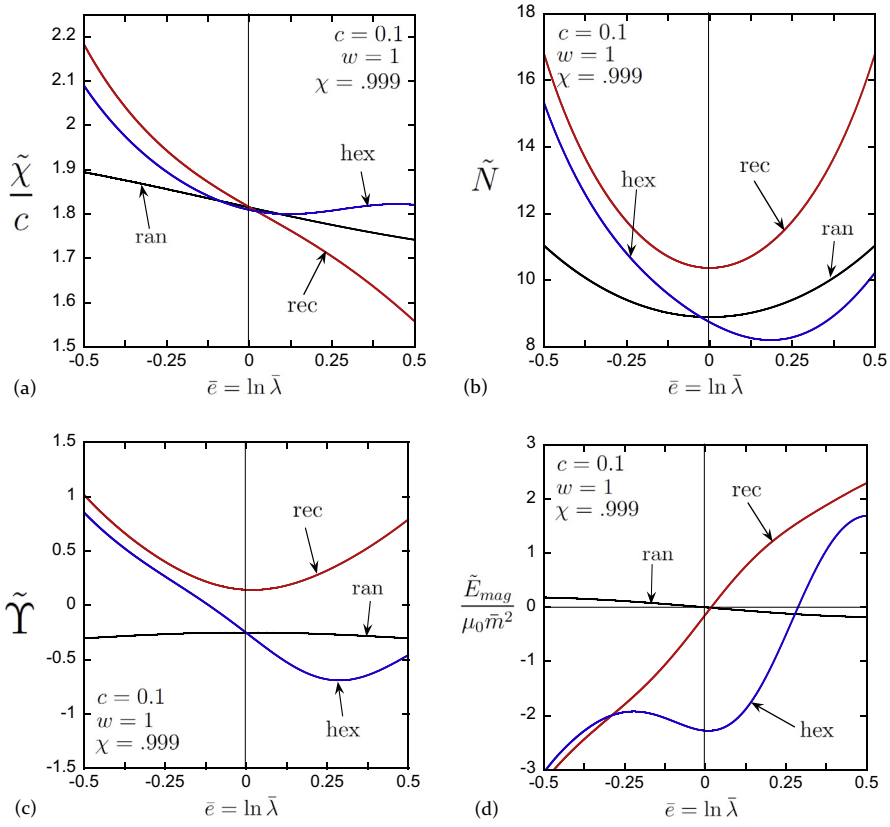

Fig. 4. Variations of the magneto-elastic properties as functions of strain for $c = 0.1$ and $w = 1$. (a) Normalized effective susceptibility. (b) Normalized mechanical stress concentration. (c) Magneto-elastic coupling coefficient. (d) Normalized magneto-elastic tangent Young's modulus.

To highlight the influence of the particle shape on the magneto-mechanical coupling, in Fig. 7 we examine the variations of the four parameters with the particle aspect ratio. Although the results are presented for composites with volume fraction $c = 0.1$, we emphasize that the trends are similar for other volume fractions. More specifically, we studied the dependence of the parameters on the aspect ratio in the range $0.01 \leqslant c \leq 0.2$ and observed only a small effect of the volume fraction in the curves shown in Fig. 7.

It is worth noting that there are qualitative similarities between the variations shown in Fig. 7 for the four parameters as functions of the aspect ratio, and the corresponding variations shown in Fig. 4 as functions of the stretch. This can be explained by observing that the relative positions of the particles are similar at different combinations of the stretch and aspect ratios. For example, the case $w = 1$ at $\bar{\lambda} = 1.2$ and the case $w = 1.44$ at $\bar{\lambda} = 1$. For random microstructures, this is explicit since $\tilde{\Upsilon}$ depends only on the quantity $w\bar{\lambda}^2$. For the periodic composites, the aspect ratio of the unit cell in the deformed configuration is $w\bar{\lambda}^2$, and we conjecture that this is the reason for the similarities in the trends of the four parameters. The fact that this similarity is observed for different shapes of the cross-sections, reinforce the observation that the magneto-elastic effects are primarily controlled by the distribution of the particles and, to a lesser extent, by the precise shape of the inclusions. This is unlike the mechanical reinforcement, which strongly depends on the particle shape.

To gain a broader view of the influence of the microstructural parameters on the macroscopic coupled response, we examine next the variations of the tractions and the deformations induced by the magnetic field. In Fig. 8(a) and (b) the variations of the actuation traction, normalized by the shear modulus of the matrix phase, are shown as functions of the fibers concentration and the aspect ratio, respectively. The precise numerical values used to determine these plots are listed in the figures. Not surprisingly, the magnitudes of the traction in the direction of the applied magnetic field increase monotonically with the volume fraction of the magnetic inclusions. However, the specific trends are dictated by the microstructure. The random composites develop compressive forces whereas the rectangular composites develop tensile forces thanks to the strong interactions between the inclusions. Depending on their distribution, the hexagonal composites may generate tensile or compressive tractions with $w = 4$ or $w = 1/4$, respectively. Interestingly, for volume fractions smaller than 0.1, the compressive tractions that develop in the random composites with $w = 4$ are larger than those that develop in the hexagonal composites with similar aspect ratio. However, the effects decay to zero in the dilute limit, in agreement with earlier comments.

As can be seen in Fig. 8(b), the dependence of the traction on w is non-monotonic, contrary to the monotonic dependence on the concentration. Here too, the tractions in the random and the rectangular composites are, respectively, compressive and tensile throughout the entire range of w. For the rectangular composites, the smallest forces are attained with a circular distribution ($w = 1$) and increase as w is varied toward higher or lower values. The compressive tractions in the random composites monotonically increase with w. The variations of the magnetically induced traction in the hexagonal composites are more complicated, from tensile to compressive as $\ln w$ changes from negative to positive values. Moreover, the compressive tractions attain a maximum at $w \approx 2.5$ and decrease beyond that point.

Next, Fig. 9 shows plots of the magnetostriction as functions of the concentration and aspect ratio for the three different distributions, respectively. In agreement with our expectations, a comparison of Fig. 9(a) with Fig. 8(a) reveals that in those composites with tensile actuation traction the magnetostriction is compressive and

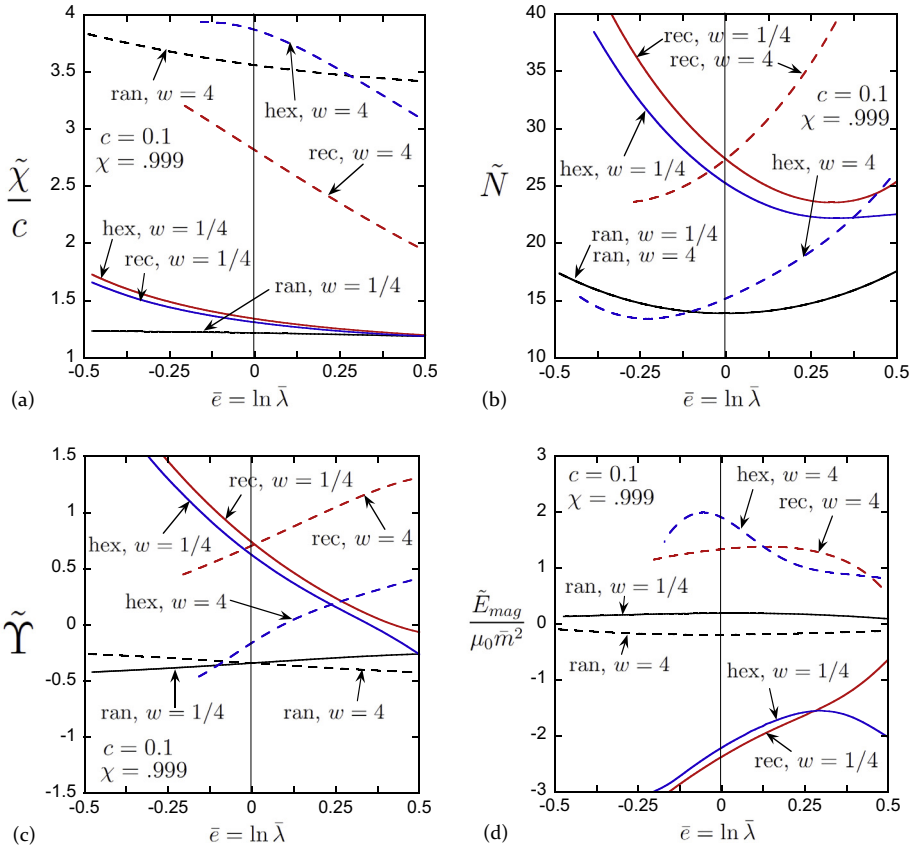

Fig. 5. Variations of the magneto-elastic properties as functions of the logarithmic strain for $c = 0.1, w = 4$ and $1/4$. (a) Normalized effective susceptibility. (b) Normalized mechanical stress concentration. (c) Magneto-elastic coupling coefficient. (d) Normalized magneto-elastic tangent Young's modulus.

vice versa. The magnetostriction is quadratic to leading order with respect to the concentration; however, as the concentration becomes large enough it is expected that the composites mechanically stiffen. This effect can be readily observed in connection with the rectangular composites with $w = 4$. For these composites, the maximal strain is attained at $c \approx 0.12$, and beyond this value the magnetostrictive strains decrease. This is in spite of the fact that the actuation traction is larger in composites with larger volume fraction of the fibers. The reason is the competition between the mechanical stiffness and the magnetic forces. Another aspect related to this competition between the two mechanisms can be traced, for example, through a comparison between the curves for the random and the hexagonal composites with $w = 4$. The curves for the actuation tractions in Fig. 8(a) suggest that the intensity of the compressive tractions in these two composites are quite similar. However, the corresponding curves in Fig. 9(a) reveal that the magnetostriction in the random composite is almost three times the one exhibited by the hexagonal composite.

Correspondingly, Fig. 9(b) shows plots of the magnetostrictive strains as functions of the aspect ratio w for three different volume fractions of the inclusion $c = 0.05, 0.10$, and 0.15. For all microstructures, almost throughout the entire range of w, larger volume fractions of the fibers lead to larger magnetostriction. Moreover, within this range of w, the strains of the rectangular and random composites monotonically increase for $w > 1$. We expect that eventually the composites will become mechanically rigid as w becomes large and the mechanical interactions will limit the magnetostrictive deformation. For the rectangular composite with $c = 0.15$, already at $w = 4$ a flattening of the curve can be identified. The curves for the hexagonal composites are more complicated, where the strains switch sign as the shape and the distribution of the fibers switches from oblate to prolate. We also note that, in agreement with the curves depicted in Fig. 8(b), the strains diminish with a decrease in the axial magnetic tractions.

Finally, to further highlight the role of the microstructure and to provide additional insights into the above-discussed findings, we provide a qualitative discussion of the results for the magnetomechanical coupling in terms of the interactions and the forces that develop between the magnetic inclusions. We begin by recalling that the interactions between pairs of magnetized particles depend on their orientation relative to the applied magnetic field (Borcea and Bruno, 2001). For simplicity, let us treat the magnetization of each particle as a dipole aligned along the $\hat{\mathbf{e}}_1$ axis due to the applied magnetic field along this direction. In particular, consider the mutual forces between pairs of magnetic spheres separated by a distance, as shown in Fig. 10. These attractive or repulsive forces among the particle pairs generate stresses in the matrix surrounding the particles that eventually lead to the macroscopic magneto-elastic effects.

The complicated nature of the inter-particle forces gives rise to the different types of coupling observed in the rectangular, hexagonal and random composites. When the particles interact along the magnetization direction as shown in Fig. 10 pair "1", they attract each other along the applied field direction. When the particles interact transverse to the applied magnetic field as in pair "5", a repulsive force is generated. At other angles, as illustrated for pairs "2", "3" and "4", the directions of the forces are different and depend on the angle with the direction of the applied field. In some configurations the particles may repel each other in the applied field direction and attract each other in the transverse direction, thus exhibiting a response opposite to the one exhibited by pairs "1" and "5".

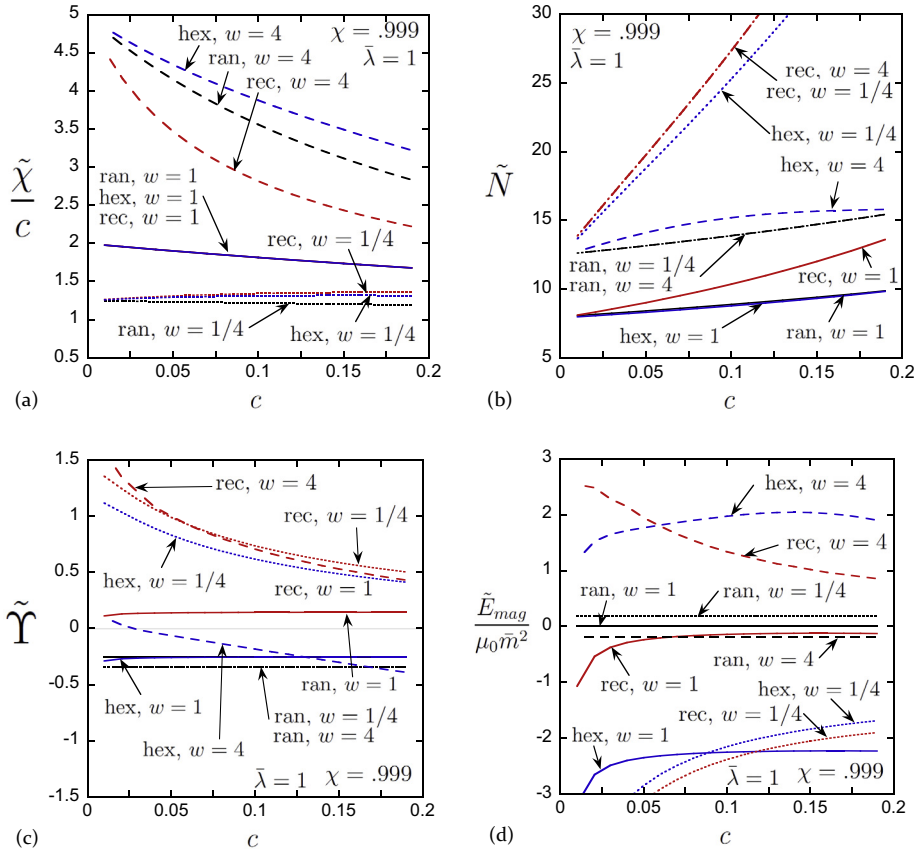

Fig. 6. Variations of the magneto-elastic properties as functions of concentration for $w = 1, 4$ and $1/4$. (a) Normalized effective susceptibility. (b) Normalized mechanical stress concentration. (c) Magneto-elastic coupling coefficient. (d) Normalized magneto-elastic tangent Young's modulus.

These interactions can shed light on the coupling observed for the three types of microstructures considered in this work. For the rectangular composites, the nearest neighbors, and therefore the dominant interactions, are of the aligned and transverse types (pairs "1" and "5"). Since the overall composite is incompressible, both types of interactions cause the composite to contract in the direction of the magnetic field. This leads to a positive magneto-elastic coupling coefficient $\tilde{\Upsilon}$ and magnetostriction effects that tend to shorten the specimen in the field direction. The interactions of pairs "1" and "5" are the dominant ones for this microstructure regardless of the initial aspect ratio and the stretch. This implies that the magnetic field always contracts these composites, resulting in a compressive tractions.

For the hexagonal composites, the dominant interactions depend on the initial aspect ratio and the deformation. At moderate values of w, where interactions of types "2", "3" and "4" dominate, the magnetic forces result in a negative magneto-elastic coupling coefficient. However, at small and large w interactions of type "1" and "5" dominate, $\tilde{\Upsilon}$ is positive, and the magnetic field causes the composite to contract. To complete the picture we recall that large deformations change the aspect ratio of the unit cell in the deformed configuration. Therefore, the nearest neighbors and the dominant inter-particle interactions may change. In turn, this may alter both the sign and the magnitude of the magneto-elastic coupling coefficient as the composite deforms. This can be tracked in Figs. 4(c) and 5(c) that show the variations of $\tilde{\Upsilon}$ for hexagonal composites with $w = 1$ and 4. Moreover, while in the case of circular fibers $\tilde{\Upsilon}$ becomes negative in passing from compressive to tensile deformations, the magneto-elastic coupling coefficient of the composite with $w = 4$ exhibits the opposite trend.

In the random composites, the particles interactions are in all possible directions, and the effective properties are determined by the average of all these interactions. Owing to this complicated interaction pattern, the magneto-elastic coupling coefficient is relatively small for this type of composites.

6. Concluding Remarks

In this work we examined the effective behavior of magnetoactive elastomers with random and periodic distributions of magnetic particles, subjected to combined magnetic and mechanical loadings that are aligned with the anisotropy axes of the MAEs (if anisotropic). To study the behavior of MAEs with periodic microstructures, we constructed finite element models and determined the effective properties of the periodic MAEs with rectangular and quasi-hexagonal microstructures. To characterize the behavior of MAEs with random microstructures we employed a recently developed theoretical homogenization framework for MAEs (Ponte Castañeda and Galipeau, 2011), and specified the results for the considered magnetomechanical loading. Thus, closed-form expressions for the MAEs response were obtained. In both analyses the effects of the magnetic Maxwell stress both inside and outside the material were accounted for.

Motivated by the potential application of these materials as "linear actuators," we specifically examined the case of uniaxial loading in the presence of a magnetic field. We introduce specific parameters that characterize the magnetomechanical performance of the MAEs. These parameters, including the magneto-elastic coupling coefficient, are used in the analysis of the magnetoactive composites. The effective parameters for three representative

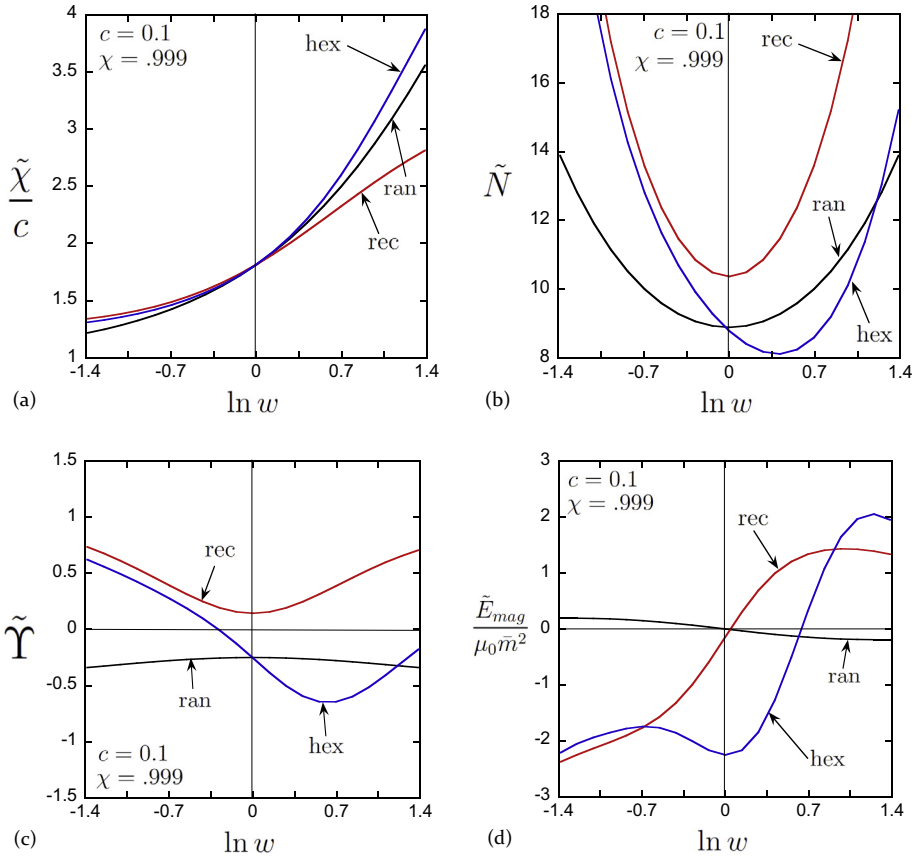

Fig. 7. Variations of the magneto-elastic properties as functions of the aspect ratio for $c = 0.1$. (a) Normalized effective susceptibility. (b) Normalized mechanical stress concentration. (c) Magneto-elastic coupling coefficient. (d) Normalized magneto-elastic tangent Young's modulus.

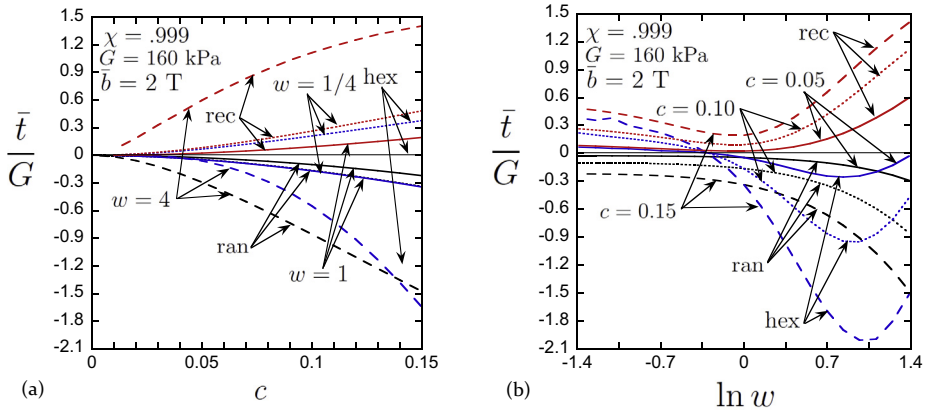

Fig. 8. Variations of the actuation traction, normalized by the matrix shear modulus, as functions of (a) the concentration of the fibers and (b) the aspect ratio of the elliptical distribution and cross-section of the fibers.

types of composites, one with random microstructure, one with rectangular and one with quasi-hexagonal, were determined. The roles of the deformation, the concentration, and the distribution and the shape of the particles on these parameters were determined, compared and analyzed.

At the macroscopic level, we distinguish between the total forces or tractions that the MAE composites generate in response to an applied magnetic field, and the total deformation or magnetostriction they undergo. The latter is essentially the result of two competing mechanisms. On the one hand, an increase in the volume fraction of the inclusions leads to an increase in the magnetic forces between them. On the other hand, an increase in the volume fraction of the inclusions also contributes to the stiffening of the composite, and hence to the reduction of the magnetically induced strains. This microstructure-induced interplay between the two competing mechanisms was previously noted by Galipeau and Ponte Castañeda (2012), as well as by Tian et al. (2012) in the context of electromechanical composites. Here, we have shown that, in some cases, composites with lower magnetically induced stresses may undergo larger magnetostriction.

We emphasize, however, that the essential variable is the magnetically induced stress which is controlled by the magneto-elastic coupling coefficient. This variable is determined not only by the magnetic susceptibility, but also, crucially, by its derivative with

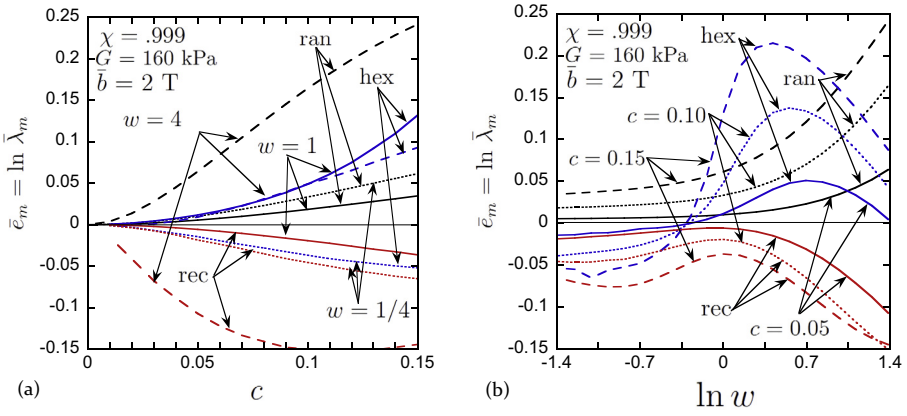

Fig. 9. Variations of the magnetostriction as functions of (a) the concentration of the fibers and (b) the aspect ratio of the elliptical distribution and cross-section of the fibers.

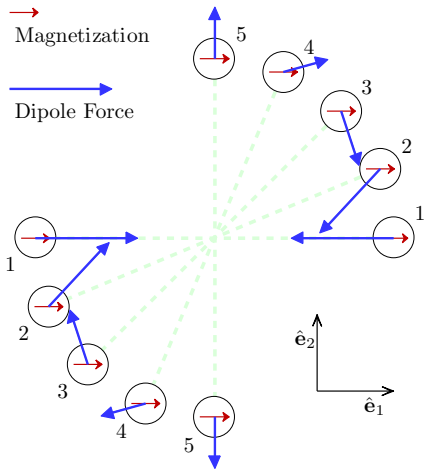

Fig. 10. The forces due to the interactions between pairs of magnetic dipoles oriented at different directions relative to the applied magnetic field. The arrows represent the forces between pairs of particles marked with similar numbers. The pairs are assumed to be sufficiently far from all other particles.

respect to the deformation. By evaluating the magnetostriction and the magneto-elastic modulus for composites with random, quasi-hexagonal, and rectangular distributions, we demonstrated that the magneto-elastic effects are of second order in the concentration. This is consistent with the fact that the coupled magnetic stresses are due to the interactions between the inclusions. In turn, we conclude that the microstructure provides the key for optimizing the magneto-elastic performance of MAEs.

Acknowledgments

The work was supported by the United States - Israel Binational Science Foundation (BSF) under the Research Grant 2008419. PPC also acknowledges support by the National Science Foundation under Grant No. CMMI-1068769.

References

Bednarek, S., 1999. The giant magnetostriction in ferromagnetic composites within an elastomer matrix. Appl. Phys. A Mater. Sci. Process. 68, 63–67.
Bertoldi, K., Gei, M., 2011. Instabilities in multilayered soft dielectrics. J. Mech. Phys. Solids 59, 18–42.
Borcea, L., Bruno, O., 2001. On the magneto-elastic properties of elastomer-ferromagnet composites. J. Mech. Phys. Solids 49, 2877–2919.
Brigadnov, I., Dorfmann, A., 2003. Mathematical modeling of magneto-sensitive elastomers. Int. J. Solids Struct. 40, 4659–4674.
Brown, W., 1966. Magneto-elastic Interactions. Springer-Verlag, New York.
Bustamante, R., Dorfmann, A., Ogden, R., 2008. On variational formulations in nonlinear magnetoelastostatics. Math. Mech. Solids 13, 725–745.
Coleman, B.D., Noll, W., 1963. The thermodynamics of elastic materials with heat conduction and viscosity. Arch. Ration. Mech. Anal. 13, 167–178.
Danas, K., Kankanala, S.V., Triantafyllidis, N., 2012. Experiments and modeling of iron-particle-filled magnetorheological elastomers. J. Mech. Phys. Solids 60, 120–138.
deBotton, G., Tevel-Deree, L., Socolsky, D.A., 2007. Electroactive heterogeneous polymers: analysis and applications to laminated composites. Mech. Adv. Mater. Struct. 14, 13–22.
Dorfmann, A., Ogden, R., 2004a. Nonlinear magnetoelastic deformations. Q. J. Mech. Appl. Math. 57, 599–622.
Dorfmann, A., Ogden, R., 2004b. Nonlinear magnetoelastic deformations of elastomers. Acta Mech. 167, 13–28.
Eshelby, J., 1957. The determination of the elastic field of an ellipsoidal inclusion and related problems. Proc. R. Soc. London A 241, 376–396.
Galipeau, E., Ponte Castañeda, P., 2012. The effect of particle shape and distribution on the macroscopic behavior of magnetoelastic composites. Int. J. Solids Struct. 49, 1–17.
Galipeau, E., Ponte Castañeda, P., 2013a. A finite-strain constitutive model for magnetorheological elastomers: magnetic torques and fiber rotations. J. Mech. Phys. Solids 61, 1065–1090.
Galipeau, E., Ponte Castañeda, P., 2013b. Giant field-induced strains in magnetoactive elastomer composites. Proc. R. Soc. London A 469, 20130385.
Geymonat, G., Müller, S., Triantafyllidis, N., 1993. Homogenization of nonlinearly elastic materials, microscopic bifurcation and macroscopic loss of rank-one convexity. Arch. Ration. Mech. Anal. 122, 231–290.
Ginder, J.M., Clark, S.M., Schlotter, W.F., Nichols, M.E., 2002. Magnetostrictive phenomena in magnetorheological elastomers. Int. J. Mod. Phys. B 16, 2412–2418.
Guan, X., Dong, X., Ou, J., 2008. Magnetostrictive effect of magnetorheological elastomer. J. Magn. Magn. Mater. 320, 158–163.
Jolly, M.R., Carlson, J.D., Munoz, B.C., 1996. A model of the behaviour of magnetorheological materials. Smart Mater. Struct. 5, 607–614.
Kankanala, S.V., Triantafyllidis, N., 2004. On finitely strained magnetorheological elastomers. J. Mech. Phys. Solids 52, 2869–2908.
Kovetz, A., 2000. Electromagnetic Theory. Oxford University Press, New York.
Lopez-Pamies, O., Ponte Castañeda, P., 2006a. On the overall behavior, microstructure evolution, and macroscopic stability in reinforced rubbers at large deformations: I—Theory. J. Mech. Phys. Solids 54, 807–830.
Lopez-Pamies, O., Ponte Castañeda, P., 2006b. On the overall behavior, microstructure evolution, and macroscopic stability in reinforced rubbers at large deformations: II — Application to cylindrical fibers. J. Mech. Phys. Solids 54, 831–863.
Maugin, G., Eringen, A., 1972. Deformable magnetically saturated media. I. Field equations. J. Math. Phys. 13, 143–155.
Maxwell, J.C., 1873. A Treatise on Electricity and Magnetism. Clarendon Press.
Michel, J.C., Lopez-Pamies, O., Ponte Castañeda, P., Triantafyllidis, N., 2010. Microscopic and macroscopic instabilities in finitely strained fiber-reinforced elastomer. J. Mech. Phys. Solids 58, 1776–1803.
Ponte Castañeda, P., Galipeau, E., 2011. Homogenization-based constitutive models for magnetorheological elastomers at finite strain. J. Mech. Phys. Solids 59, 194–215.
Ponte Castañeda, P., Siboni, M.H., 2012. A finite-strain constitutive theory for electro-active polymer composites via homogenization. Int. J. Nonlinear Mech. 47, 293–306.
Ponte Castañeda, P., Willis, J., 1995. The effect of spatial distribution on the effective behavior of composite materials and cracked media. J. Mech. Phys. Solids 43, 1919–1951.

Rudykh, S., Bertoldi, K., 2013. Stability of anisotropic magnetorheological elastomers in finite deformations: a micromechanical approach. J. Mech. Phys. Solids 61, 949–967.
Rudykh, S., deBotton, G., 2011. Stability of anisotropic electroactive polymers with application to layered media. Z. Angew. Math. Phys. 62, 1131–1142.
Rudykh, S., deBotton, G., 2012. Instabilities of hyperelastic fiber composites: micromechanical versus numerical analyses. J. Elast. 106, 123–147.
Rudykh, S., Lewinstein, A., Uner, G., deBotton, G., 2013. Analysis of microstructural induced enhancement of electromechanical coupling in soft dielectrics. Appl. Phys. Lett. 102, 151905.
Rudykh, S., Bhattacharya, K., deBotton, G., 2014. Multiscale instabilities in soft heterogeneous dielectric elastomers. Proc. Roy. Soc. A 470, 20130618.
Siboni, M.H., Ponte Castañeda, P., 2013. Dielectric elastomer composites: small-deformation theory and applications. Philos. Mag. 93, 2769–2801.
Tian, L., Tevet-Deree, L., deBotton, G., Bhattacharya, K., 2012. Dielectric elastomer composites. J. Mech. Phys. Solids 60, 181–198.
Tiersten, H., 1964. Coupled magnetomechanical equations for magnetically saturated insulators. J. Math. Phys. 5, 1298–1318.
Toupin, R., 1956. The elastic dielectric. J. Ration. Mech. Anal. 5, 849–915.
Truesdell, C., Toupin, R., 1960. The classical field theories. In: Handbuch der Physik III. Springer, Berlin.
Vu, D., Steinmann, P., 2007. Nonlinear electro- and magneto-elastostatics: material and spatial settings. Int. J. Solids Struct. 44, 7891–7905.
Yin, H.M., Sun, L.Z., 2006. Magnetoelastic modelling of composites containing randomly dispersed ferromagnetic particles. Philos. Mag. 86, 4367–4395.
Yin, H.M., Sun, L.Z., Chen, J.S., 2006. Magneto-elastic modeling of composites containing chain-structured magnetostrictive particles. J. Mech. Phys. Solids 54, 975–1003.